Available online at www.sciencedirect.com
ScienceDirect
Thermochimica Acta 448 (2006) 123–129
thermochimica acta
www.elsevier.com/locate/tca

DSC study and computer modelling of the melting process in ice slurry

T. Kousksou*, A. Jamil, Y. Zeraouli, J.-P. Dumas

Laboratoire de Thermique Énergétique et Procédés, Avenue de l'Université, BP 1155, 64013 Pau Cedex, France

Received 6 March 2006; received in revised form 26 June 2006; accepted 12 July 2006
Available online 18 July 2006

Abstract

In order to understand the non-isothermal melting kinetics in the ice slurry, a differential scanning calorimetry (DSC) was used. Experimental results were compared to those obtained by a numerical simulation in which a general enthalpy method was applied. In this work the ice slurry studied consists of ice particles uniformly dispersed within a water–antifreeze liquid mixture. The effects of the heating rate and the initial antifreeze mass fraction are discussed. It has been found that the temperature gradients inside the sample of the solution become important if either heating rate increases or initial antifreeze mass fraction decreases.

Keywords: Heat transfer; Ice/water–ethanol; Ice slurry; DSC; Simulation

1. Introduction

Nowadays, considerable work for the development on the ice–liquid mixtures (or ice slurries) is under way in many countries [1]. The ice slurry studied consists of ice particles uniformly dispersed within a water–antifreeze liquid mixture. The main benefit of using ice slurry is the latent heat of ice or enthalpy difference at melting [2,3]. Ice slurries have several times higher heat transport capability than single-phase fluids. Due to this and its more complex behaviour, ice slurry is sometimes referred to as advanced secondary fluid.

Because of its good thermophysical and technological characteristics, ethanol–water solution is one of the most studied mixture. In the literature [4–7] there is a great information on the diphasic properties.

For design and performance evaluation of a thermal storage system using ice slurry, it is necessary to understand the behavior of the ice slurry during the phase change process.

The issue of heat transfer during melting of ice in ice slurries has been a subject for several papers. Their review is given in Refs. [8,2]. In these works, special attention has been paid to the determination of the values of heat transfer coefficients.

The aim of the present contribution is to investigate, experimentally and numerically, the kinetics of the melting of ice slurry in the small container by using the differential scanning calorimetry (DSC). The influences of both initial antifreeze mass fraction and heating rate were investigated.

2. Binary phase diagram

The phase diagram of the aqueous binary solution of ethanol [9] is presented in Fig. 1.

In our application, the eutectic point and over-eutectic part are not of interest, because the ice slurry is available in the temperatures range from just below 0 to −20 °C.

The ice mass fraction is calculated from the melting temperature T of the binary mixture solution, which is a function of the ethanol mass fraction W_a in the residual liquid solution:

$$T = T(W_a) \tag{1}$$

Once the initial mass fraction of ethanol in the binary mixture solution before freezing $W_{a,i}$ and the temperature are known, the equilibrium ice mass fraction is calculated with:

$$W_{ic}(T) = 1 - \frac{W_{a,i}}{W_a(T)} \tag{2}$$

in which $W_a(T)$ is found from the liquidus curve, the inverse of Eq. (1).

* Corresponding author.
E-mail address: Tarik.kousksou@univ-pau.fr (T. Kousksou).

0040-6031/$ – see front matter © 2006 Elsevier B.V. All rights reserved.
doi:10.1016/j.tca.2006.07.004

Nomenclature

ΔA	area (m^2)
c	specific heat capacity ($J\,kg^{-1}\,K^{-1}$)
h	heat transfer coefficient ($W\,m^{-2}\,K^{-1}$)
H	massic enthalpy ($J\,kg^{-1}$)
L_f	Latent heat of ice ($J\,kg^{-1}$)
t	time (s)
Δt	time step (s)
T	temperature (°C)
T_{peak}	peak maximum temperature (°C)
V	volume (m^3)
W	mass fraction

Greek symbols

β	heating rate ($°C\,min^{-1}$)
λ	thermal conductivity ($W\,m^{-1}\,K^{-1}$)
ρ	density ($kg\,m^{-3}$)
φ	volume fraction of ice
Φ	specific heat flow rate ($W\,kg^{-1}$)

Subscripts

a	antifreeze
i	initial
ic	ice
l	liquid
mix	mixture
nb	neighbor nodes of P
P	node point P
plt	plate
ref	reference
w	water

Superscripts

m	iteration level
old	previous time step value

3. Differential scanning calorimetry (DSC)

The principle of the power-compensation used in the DSC is that the temperatures of the sample and reference are controlled independently using separate, identical furnaces (Fig. 2). Even in case of thermal event for the sample, the temperatures of the plates containing the sample and the reference are maintained identical. The thermogram is Φ the difference of power required to maintain this equality:

$$\Phi = (\Phi)_{sample} - (\Phi)_{ref} \quad (3)$$

As indicated in Refs. [10,11], the power exchanged at the reference plate is practically constant and equal to $(\Phi)_{ref} = \beta c_{ref}$, where c_{ref} is the specific heat of the reference cell and β is the heating rate. So to simplify the model we will omit the second term from the calculation of Φ.

The DSC experiments were conducted by placing approximately 11 mg of the solution (water–ethanol) in the aluminum DSC cell. The sample was cooled at 2 °C/min until ice formed in the solution, typically at −30 °C (observed as a sharp exothermic peak on the DSC thermogram). The sample was then re-equilibred at this temperature (−30 °C) for 3–5 min. Isothermal equilibrium at the phase change temperature will permit the ice crystals to be in equilibrium with the solution. The sample was then heated at various scan rates β from −30 to +10 °C, to obtain the thermograms.

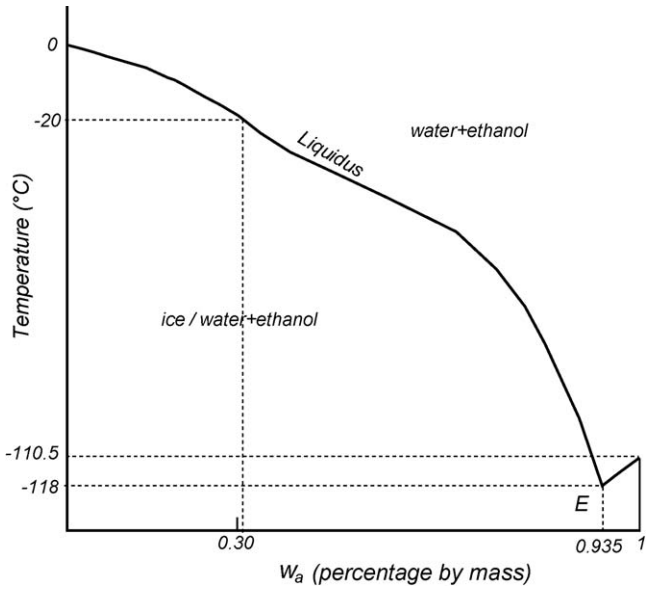

Fig. 1. Phase diagram of the aqueous binary solution of ethanol.

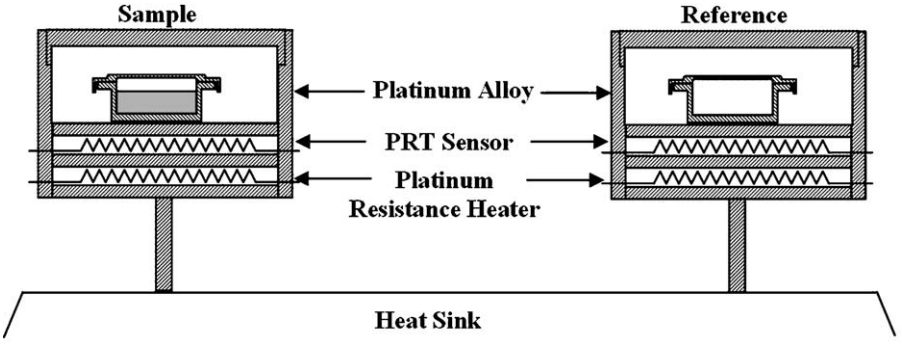

Fig. 2. Scheme of the calorimeter head.

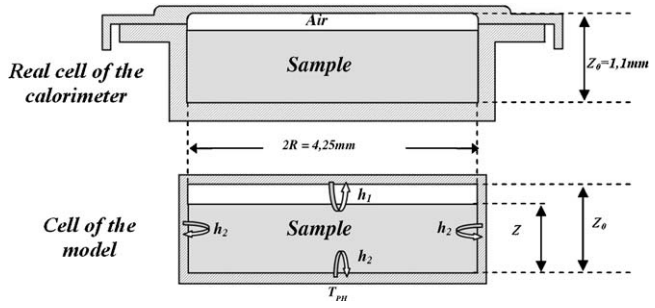

Fig. 3. Experiment cell and scheme for the model.

Recent studies in our laboratory [12] and elsewhere [13] have demonstrated that at the crystallization (supercooling breakdown) there is the constitution of small dendrites of ice and the mixture formed has the structure of slurries described in Section 1 and object of our research.

4. Physical model and basic equations

In Fig. 3 we have drawn the actual cell and the simplified scheme used in our model. The binary mixture solution (ice/water–ethanol) fills a cylindrical cell of height $Z_0 = 1.1$ mm and radius $R = 2.125$ mm.

The following assumptions are used in the design of the numerical simulation model:

- The ice consists of pure water.
- The diphasic medium is considered as a slurry ice whose properties are given by combining properties of the liquid solution and those of pure ice.
- The ice particles are supposed uniformly dispersed in the sample. Each ice particle is locally in equilibrium with the close solution.
- Because of the small dimensions of the sample, the convection effects due to density change at the phase change interface are neglected.

Under the foregoing assumptions, the partial differential equation governing the energy is:

$$\frac{\partial[\rho H]}{\partial t} = \nabla \cdot (\lambda \nabla T) \tag{4}$$

To account for the latent heat effect in the phase change, occurring over a finite range of temperatures, the general enthalpy method of Swaminathan and Voller [14–16] is adopted.

The total enthalpy ρH for the unit volume is given by the weighted sum of sensible enthalpies of the solid and liquid phases and the latent heat effect:

$$\rho H = (1 - W_{ic})\rho_l H_l + W_{ic}\rho_{ic} H_{ic} \tag{5}$$

where ρ_{ic} and ρ_l are the ice and liquid volume densities, H_{ic} and H_l are the ice and liquid mass enthalpy and W_{ic} is the ice mass fraction.

The enthalpy of ice and water–antifreeze liquid mixture can be evaluated from a heat balance performed on the ice slurry mixture neglecting the enthalpy of dilution of the mixture [17] and using as reference the enthalpy of the liquid at 0 °C ($H_{l,T=0\,^\circ C} = 0$ kJ/kg). Thus, the massic enthalpy of ice can be calculated as:

$$H_{ic} = -L_f + \int_0^T c_{ic}(\theta)\,d\theta \tag{6}$$

The massic enthalpy of the liquid phase H_l depends on the ethanol concentration and on the temperature:

$$H_l = W_a \int_0^T c_a(\theta)\,d\theta + (1 - W_a) \times \int_0^T c_w(\theta)\,d\theta + \Delta_{mix} H_l(W_a) \tag{7}$$

where c_{ic}, c_a and c_w are the ice, antifreeze and water mass heat capacity, L_f the melting heat of ice and $\Delta_{mix} H_l(W_a)$ is the heat of mixing of the two substances.

In our model, we have supposed that the heat of mixing linked to the molecular interactions between water and ethanol in liquid phase is negligible [18,19].

In order to determine the conductivity of the ice slurry we have selected the Maxwell relation [20], because it provides satisfactory results in our model:

$$\lambda = \lambda_l \frac{2\lambda_l + \lambda_{ic} - 2\varphi(\lambda_l - \lambda_{ic})}{2\lambda_l + \lambda_{ic} - \varphi(\lambda_l - \lambda_{ic})} \tag{8}$$

where λ_l and λ_{ic} are the thermal conductivities of solution and ice [21,7] and φ is the volume fraction of ice in the slurry given by the following expression:

$$\varphi = W_{ic}\frac{\rho}{\rho_{ic}} \tag{9}$$

The substitution of Eqs. (5)–(7) into Eq. (4) leads to the temperature-source based on the energy equation used in this work:

$$\frac{\partial[\rho c T]}{\partial t} = \nabla \cdot (\lambda \nabla T) + \rho_{ic} L_f \frac{\partial W_{ic}}{\partial t} \tag{10}$$

where

$$\rho c = (1 - W_{ic})\rho_l c_l + W_{ic}\rho_{ic} c_{ic} \tag{11}$$

and c_l is the water–ethanol mass heat capacity [7,6].

Initial and boundary conditions

At $t = 0$ the temperature of the binary mixture solution is known. The ethanol mass fraction W_a can be determined from the liquidus curve and the equilibrium ice mass fraction is calculated from Eq. (2).

Due to the higher thermal conductivity of the cell metal, it is assumed that the envelope of the sample is at the plates temperature T_{plt} and is programmed to be a linear function:

$$T_{plt} = \beta t + T_0 \tag{12}$$

We take into account the heat fluxes between the envelope and the sample and we consider two different heat exchange coefficients (Fig. 3): h_1 the heat transfer between the solution and the air in the top of the cell and h_2 the heat transfer between the

solution and both lateral and bottom surface areas of the cell. So:

$$-\lambda\left(\frac{\partial T}{\partial z}\right)_{z=Z} = h_1(T_{z=Z} - T_{\mathrm{plt}}) \tag{13}$$

$$-\lambda\left(\frac{\partial T}{\partial r}\right)_{r=R} = h_2(T_{r=R} - T_{\mathrm{plt}}) \tag{14}$$

$$-\lambda\left(\frac{\partial T}{\partial z}\right)_{z=0} = h_2(T_{z=0} - T_{\mathrm{plt}}) \tag{15}$$

A slip boundary condition is imposed on the symmetry axis:

$$\left(\frac{\partial T}{\partial r}\right)_{r=0} = 0 \tag{16}$$

Because the assumption of the high conductivity of the metallic cells, we also consider that the flux Φ which attains the plate is the sum of the thermal fluxes through each walls:

$$\begin{aligned}\Phi = &-\int_{z=0}^{z=Z} h_2(T_{r=R} - T_{\mathrm{plt}})\,\Delta A_{r=R} \\ &-\int_{r=0}^{r=R} h_2(T_{z=0} - T_{\mathrm{plt}})\,\Delta A_{z=0} \\ &-\int_{r=0}^{r=R} h_1(T_{z=Z} - T_{\mathrm{plt}})\,\Delta A_{z=Z}\end{aligned} \tag{17}$$

5. Numerical procedure

The finite difference equations are obtained upon integrating Eq. (9) over each of the control volumes as shown in bold in Fig. 4 designed as P. Because of the very small dimensions of the control volume, the ice slurry temperature is assumed to be homogeneous in it and in local equilibrium.

The resulting finite difference scheme at the time $t + \Delta t$ has the form:

$$\begin{aligned}a_{\mathrm{P}}T_{\mathrm{P}} = &\Sigma_{\mathrm{nb}}a_{\mathrm{nb}}T_{\mathrm{nb}} + \frac{\rho_{\mathrm{P}}c_{\mathrm{P}}V_{\mathrm{P}}}{\Delta t}T_{\mathrm{P}}^{\mathrm{old}} \\ &- \rho_{\mathrm{ic}}\,\Delta H\frac{V_{\mathrm{P}}}{\Delta t}\left((W_{\mathrm{ic}})_{\mathrm{P}} - (W_{\mathrm{ic}})_{\mathrm{P}}^{\mathrm{old}}\right)\end{aligned} \tag{18}$$

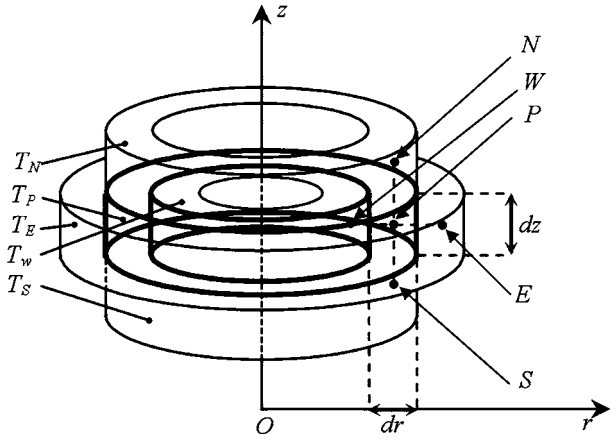

Fig. 4. Control volume.

where

$$\Sigma_{\mathrm{nb}}a_{\mathrm{nb}}T_{\mathrm{nb}} = a_{\mathrm{W}}T_{\mathrm{W}} + a_{\mathrm{E}}T_{\mathrm{E}} + a_{\mathrm{N}}T_{\mathrm{N}} + a_{\mathrm{S}}T_{\mathrm{S}} \tag{19}$$

$$a_{\mathrm{W}} = \frac{2\pi\lambda_{\mathrm{W}}r_{\mathrm{W}}\Delta z}{\Delta r} \tag{20}$$

$$a_{\mathrm{E}} = \frac{2\pi\lambda_{\mathrm{E}}r_{\mathrm{E}}\Delta z}{\Delta r} \tag{21}$$

$$a_{\mathrm{N}} = \frac{\pi\lambda_{\mathrm{N}}(r_{\mathrm{E}}^2 - r_{\mathrm{W}}^2)}{\Delta z} \tag{22}$$

$$a_{\mathrm{S}} = \frac{\pi\lambda_{\mathrm{S}}(r_{\mathrm{E}}^2 - r_{\mathrm{W}}^2)}{\Delta z} \tag{23}$$

$$a_{\mathrm{P}} = \frac{\rho_{\mathrm{P}}c_{\mathrm{P}}V_{\mathrm{P}}}{\Delta t} + a_{\mathrm{W}} + a_{\mathrm{E}} + a_{\mathrm{N}} + a_{\mathrm{S}} \tag{24}$$

$$V_{\mathrm{P}} = \pi(r_{\mathrm{E}}^2 - r_{\mathrm{W}}^2)\Delta z \tag{25}$$

V_{P} is a volume associated with the Pth node point, the subscripts P, "nb (E, W, N, S)" and "old" refer to the Pth node point, the neighboring node points, and the old time value respectively.

The Eq. (18) require a special treatment. In fact the unknowns are only the temperatures T_{P} because the mass fractions of ice W_{ic} are themselves function of the temperatures according to Eq. (2) But these equations are non-linear and the calculation of all temperatures T_{P} by an implicit method is impossible.

The principle of the resolution procedure according [15] is, knowing the results at time t (old), the determination of the temperature at time $t + \Delta t$ is given after an iteration. For the mth iteration we use a fictitious temperatures T_{P}^m and we impose a fictitious mass fractions W_{ic}^m. At the next iteration we can calculate the new temperature value T^{m+1} by the equation:

$$\begin{aligned}a_{\mathrm{P}}T_{\mathrm{P}}^{m+1} = &\Sigma_{\mathrm{nb}}a_{\mathrm{nb}}T_{\mathrm{nb}}^{m+1} + \frac{\rho_{\mathrm{P}}c_{\mathrm{P}}V_{\mathrm{P}}}{\Delta t}T_{\mathrm{P}}^{\mathrm{old}} \\ &- \rho_{\mathrm{ic}}\,\Delta H\frac{V_{\mathrm{P}}}{\Delta t}\left((W_{\mathrm{ic}}^{m+1})_{\mathrm{P}} - (W_{\mathrm{ic}})_{\mathrm{P}}^{\mathrm{old}}\right)\end{aligned} \tag{26}$$

But at each outer iteration $(m + 1)$ the solid fraction can be updated from the values at the previous outer iteration (m) through the formula:

$$(W_{\mathrm{ic}}^{m+1})_{\mathrm{P}} = (W_{\mathrm{ic}}^{m})_{\mathrm{P}} + \frac{\mathrm{d}W_{\mathrm{ic}}}{\mathrm{d}T}(T_{\mathrm{P}}^{m+1} - T_{\mathrm{P}}^{m}) \tag{27}$$

where the term $\mathrm{d}W_{\mathrm{ic}}/\mathrm{d}T$ is evaluated by deriving Eq. (2) at T_{P}^m:

$$\frac{\mathrm{d}W_{\mathrm{ic}}}{\mathrm{d}T} = \left(\frac{W_{\mathrm{a,i}}}{W_{\mathrm{a}}^2}\right)\frac{\mathrm{d}W_{\mathrm{a}}}{\mathrm{d}T} \tag{28}$$

and $\mathrm{d}W_{\mathrm{a}}/\mathrm{d}T$ is the derivation of the liquidus.

Substitution of Eq. (27) into equation Eq. (26) leads to the iterative equation:

$$\begin{aligned}&\left[a_{\mathrm{P}} + \rho_{\mathrm{ic}}\,\Delta H\frac{\mathrm{d}W_{\mathrm{ic}}}{\mathrm{d}T}\frac{V_{\mathrm{P}}}{\Delta t}\right]T_{\mathrm{P}}^{m+1} \\ &= \Sigma_{\mathrm{nb}}a_{\mathrm{nb}}T_{\mathrm{nb}}^{m+1} + \frac{\rho_{\mathrm{P}}c_{\mathrm{P}}V_{\mathrm{P}}}{\Delta t}T_{\mathrm{P}}^{\mathrm{old}} \\ &\quad + \rho_{\mathrm{ic}}\,\Delta H\frac{V_{\mathrm{P}}}{\Delta t}\left((W_{\mathrm{ic}})_{\mathrm{P}}^{\mathrm{old}} - (W_{\mathrm{ic}}^{m})_{\mathrm{P}} + T_{\mathrm{P}}^{m}\right)\end{aligned} \tag{29}$$

We stop the iterations when $\|T^{m+1} - T^m\| < \varepsilon$ and we attribute at $t + \Delta t$ the values of T^{m+1} and the mass fraction W_{ic}^{m+1}. Typically $\varepsilon = 10^{-5}$ was used.

6. Results and discussion

6.1. Thermal analysis

Thermal analyses were carried out using a PYRIS DIAMOND DSC of Perkin-Elmer. For the numerical calculation, we have applied the procedure described in the previous section. The values of physical characteristics required in the different equations have been taken in the literature [4,7], except the coefficients of heat exchange (h_1 and h_2) that have been determined by simulation from exploratory experiments.

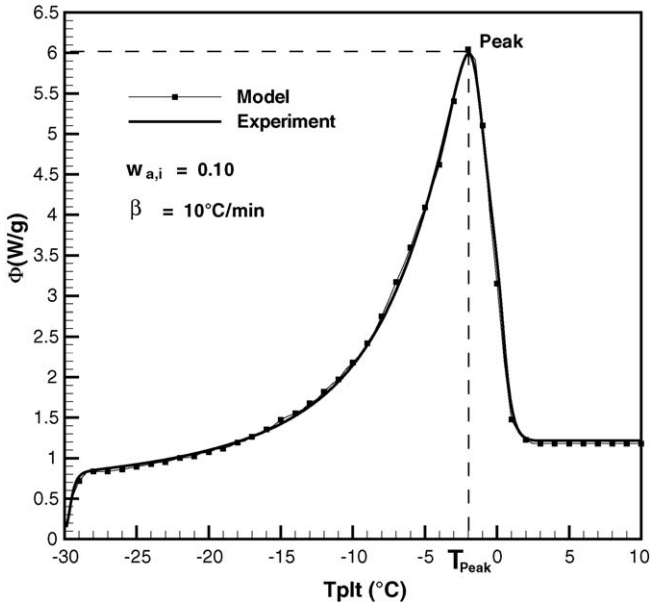

Fig. 5. Theoretical and experimental thermogram ($\beta = 10\,^{\circ}\mathrm{C\,min^{-1}}$, $W_{a,i} = 0.1$).

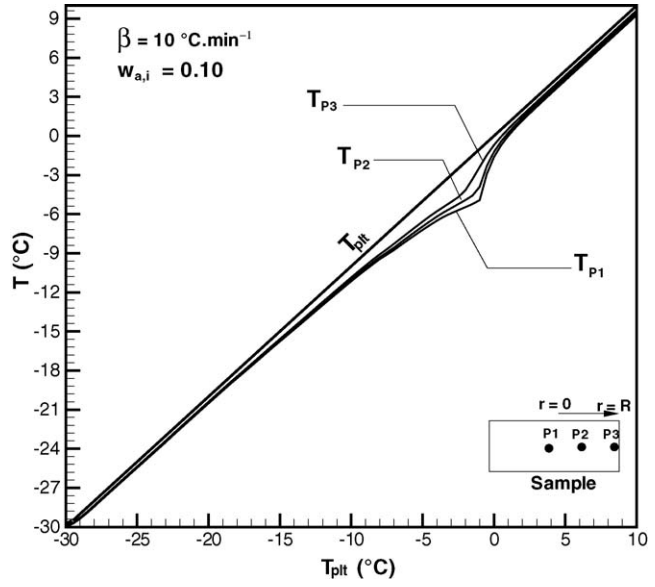

Fig. 6. Temperature vs. radius ($\beta = 10\,^{\circ}\mathrm{C\,min^{-1}}$, $W_{a,i} = 0.1$).

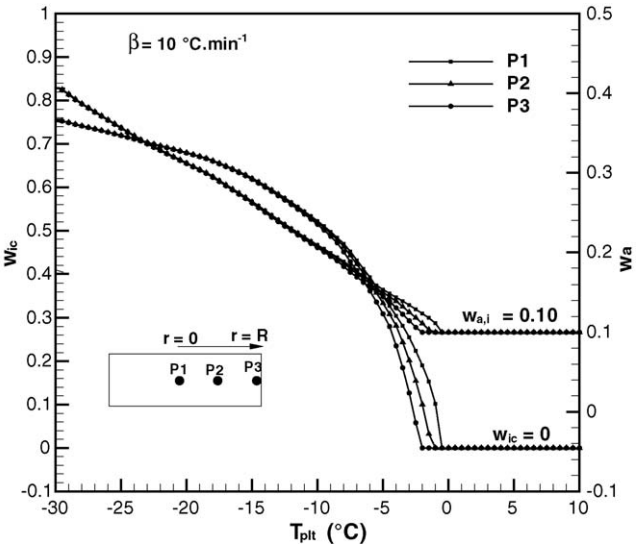

Fig. 7. W_{ic} and W_a vs. radius ($\beta = 10\,^{\circ}\mathrm{C\,min^{-1}}$, $W_{a,i} = 0.1$).

A comparison between the experimental thermogram and the calculated one is shown in Fig. 5. The fit between both thermograms is good: the rounded form of the top of the peak is reproduced and its width is the same. The observed one-peak thermogram is a clear indication of the progressive melting of the binary mixture solution.

Figs. 6 and 7 present the temperatures at different point in the sample and the corresponding mass fraction of ice versus temperature imposed on the sample T_{plt}. Fig. 7 also includes the corresponding mass fraction of ethanol versus T_{plt}. Temperature differences can be observed as a function of the radius. These differences can reach 3 °C at certain points. We can note that the temperature differences inside the sample is due to the heat con-

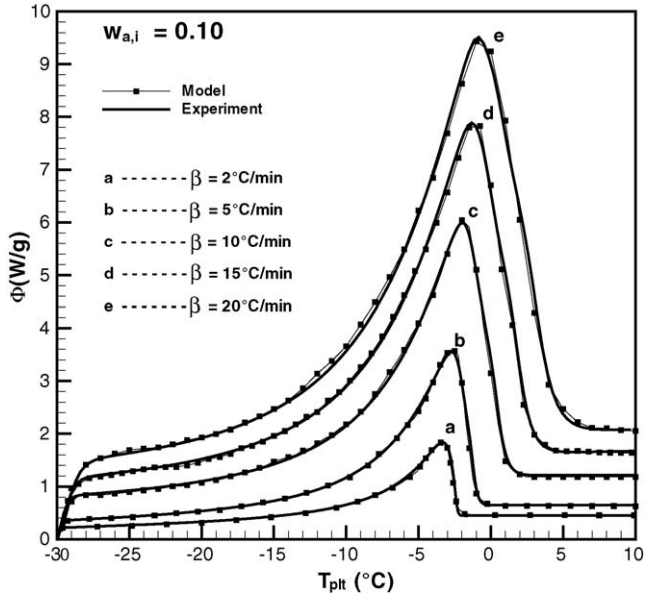

Fig. 8. Effect of the heating rate on the shape of thermograms.

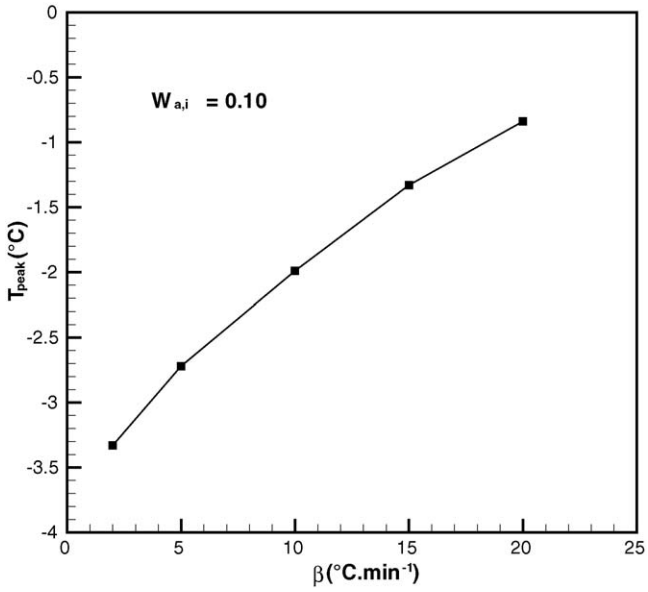

Fig. 9. Effect of the heating rate on the peak temperature.

duction within the binary mixture. The melting process finishes when the ethanol mass fraction reaches the initial mass fraction of the ethanol and we observe that in all cases this event occurs after the time of the maximum of the peak.

6.2. Effects of heating rate on the shape of thermograms

Fig. 8 shows the thermograms obtained by the model and DSC versus the heating rate β. The peak temperatures range becomes broader and it shifts to greater temperatures with increasing heating rate.

T_{peak} represents the value of the temperature of the plate when the energy exchange is maximum. The comparison of Figs. 5 and 7 shows that the maximum of the peak at T_{peak} does not represent the end of the phase change, particularly at the center of the cell. The difference is obviously due to the overall thermal resistance (both between the sample and the DSC plate form and inside the sample) and is enlarged when the heating rate β increases as it is described in Fig. 9.

Fig. 10 shows that the temperature difference inside the sample becomes more important as the heating rate increases.

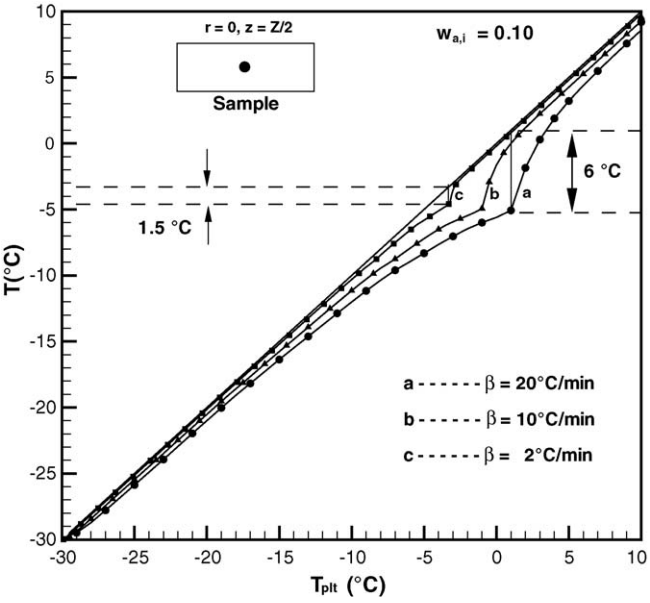

Fig. 10. Influence of the heating rate on the temperature in the centre of the sample.

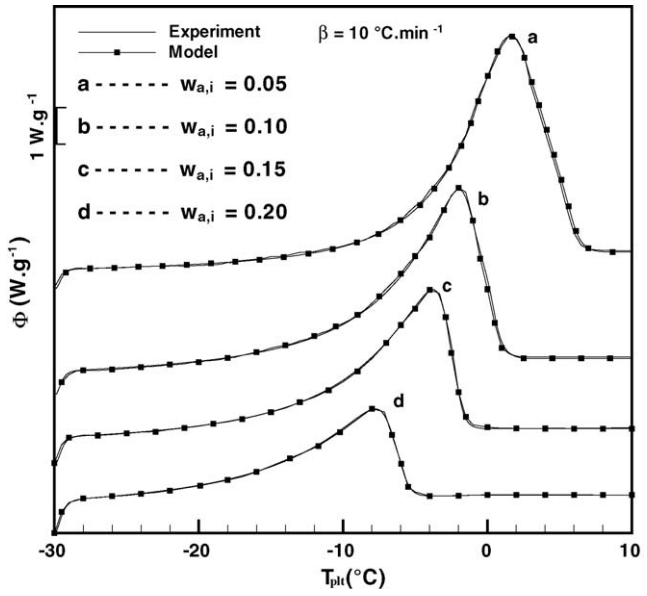

Fig. 11. Influence of the initial antifreeze mass fraction on the shape of thermograms.

6.3. Effects of the initial mass fraction of the ethanol on the shape of thermograms

From both experiments and numerical analysis, we present the heat flow Φ for each initial mass fraction of the ethanol in the binary mixture solution at a fixed heating rate, as one can

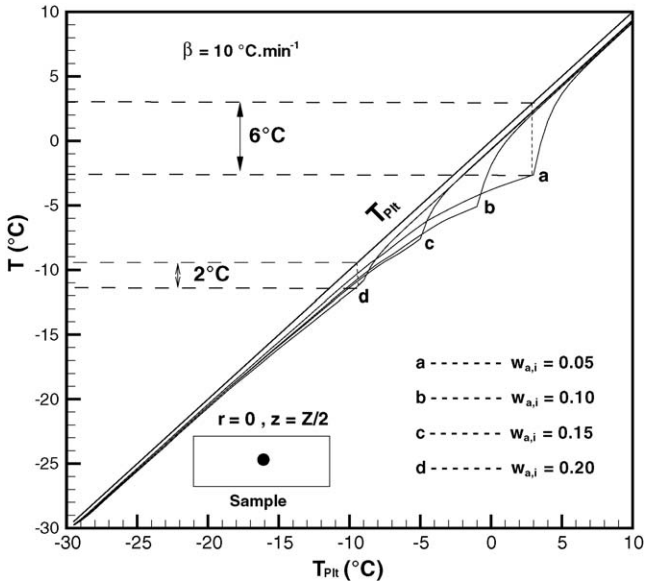

Fig. 12. Influence of the initial antifreeze mass fraction on the temperature in the center of the sample.

see in Fig. 11. In these plots we find that the peak temperature decreases with increasing initial mass fraction of ethanol since the equilibrium temperature decreases (Fig. 1).

From Fig. 12 we can observe that the temperature difference between the plate and the center of the sample becomes more important as the initial mass fraction of ethanol decreases because the power involved in the transformation is more important enhancing the heat transfers.

7. Conclusion

In this study, we have presented a two-dimensional model simulating a non-isothermal melting of the binary mixture solution (ice/water–ethanol). The good agreement between experimental and calculated thermograms has permitted a validation of the model and deduce some inaccessible values, such as the distribution of the temperature and the evolution of the ice mass fraction and the ethanol mass fraction versus the temperature imposed on the sample. The application of this model to the differential scanning calorimetry has permitted the understanding of the heat transfers inside the investigated samples.

References

[1] W. Egolf, M. Kauffeld, From physical properties of ice slurries to industrial ice slurry applications, Int. J. Refrig. 28 (2005) 164–174.
[2] W. Egolf, A. Kitanovski, D. Ata-Caesar, E. Stamatiou, M. Kawaji, J.P. Bedecarrats, F. Strub, Thermodynamics and heat transfer of ice slurries, Int. J. Refrig. 28 (2005) 51–59.
[3] A. Melinder, E. Granryd, Using property values of aqueous solutions and ice to estimate ice concentrations and enthalpies of ice slurries, Int. J. Refrig. 28 (2005) 13–19.
[4] A. Melinder, Thermophysical properties of liquid secondary refrigerants, Tables and diagrams for industry, IIR edition, 1997.
[5] O. Bel, A. Lallemand, Study of a two phase secondary refrigerant 1: intrinsic thermophysical properties of an ice slurry, Int. J. Refrig. 22 (1999) 13–19.
[6] C. Peuvrel, Etude des transferts thermiques lors de la circulation dans un changeur d'un fluide frigoporteur changement de phase solide-liquide, Thèse de doctorat, Université de Pau et des Pays de l'Adour-France, 2003.
[7] M.B. Lakhdar, Comportement thermo-hydraulique d'un fluide frigoporteur diphasique: le coulis de glace: Etude théorique et expérimentale, Thèse de doctorat, INSA Lyon-France, 1998.
[8] V. Ayel, O. Lottin, H. Peergossaini, Rheology, flow behaviour and heat transfer of ice slurries: review of the state of the art, Int. J. Refrig. 26 (2003) 95–107.
[9] I. Mellan, Industrial Solvents Handbook, Neyes Data Corporation, New Jersey, 1977, p. 133.
[10] J.P. Dumas, Y. Zeraouli, M. Strub, Heat transfer inside emulsions: determination of the DSC thermograms—Part 2, melting of the crystallized droplets, Thermochim. Acta 236 (1994) 239–248.
[11] J.P. Dumas, Y. Zeraouli, M. Strub, Heat transfer inside emulsions: determination of the DSC thermograms—Part 1, crystallization of the undercooled droplets, Thermochim. Acta 236 (1994) 227–237.
[12] P. Reghem, Etude hydrodynamique de fluides diphasiques solide-liquide en conduite circulaire: Application au coulis de glace, Thèse de doctorat, Université de Pau et des Pays de l'Adour-France, 2002.
[13] V. Ayel, O. Lottin, M. Faucheux, D. Sallier, H. Peerhossaini, Cystallization of undercooled aqueous solutions: experimental study of free dendritic growth in cylindrical geometry, Int. J. Heat Mass Transfer 49 (2006) 1876–1884.
[14] V.R. Voller, Implicit finite-difference solutions of the enthalpy formulation of Stefan problems, IMA J. Numer. Anal. 5 (1985) 201–214.
[15] V.R. Voller, C.R. Swaminathan, General source-based method for solidification phase change, Numer. Heat Transfer B 19 (1991) 175–189.
[16] V.R. Voller, C.R. Swaminathan, B.G. Thomas, Fixed grid techniques for phase change problems: a review, Int. J. Numer. Meth. Eng. 30 (1990) 875–898.
[17] J. Guilpart, E. Stamatiou, A. Delahaye, L. Fournaison, Comparison of the performance of different ice slurry types depending on the application temperature, Int. J. Refrig. 29 (2006) 781–788.
[18] O. Lottin, C. Epiard, Dependence of the thermodynamic properties of ice slurries on the characteristics of marketed antifreezes, Int. J. Refrig. 24 (2001) 445–467.
[19] M.B. Lakhdar, R. Cerecero, G. Alvarez, J. Guilpart, D. Flick, A. Lallemand, Heat transfer with freezing in a scraped surface heat exchanger, ATE 25 (2005) 45–60.
[20] J. Guilpart, Fournaison, M.B. Lakhdar, Méthode de calcul des propriétés thermophysiques des coulis de glace: application au mélange eau-éthanol, in: Proceedings of the 20th International Congress of Refrigeration, Sydney, Australia, 1999.
[21] F.L. Levy, Calculating the thermal conductivity of meat and fish in the freezing range, Revue Internationale du froid 5 (1982) 149–154.